Based on Serum Raman and Fluorescence Spectra to Diagnose Liver Cancer

Quanhong Ou
Yunnan Normal University
Xien Yang
Yunnan Normal University
Weiye Yang
Yunnan Normal University
Liqin Jiang
Yunnan Normal University
Kai Qian
The First People's Hospital of Yunnan Province
Youming Shi
Qujing Normal University
Gang Liu (gliu66@163.com)
Yunnan Normal University

Research Article

Keywords: Raman spectroscopy, Fluorescence spectroscopy, Liver cancer, Principal component analysis, Partial least squares discriminant analysis

Posted Date: January 12th, 2022

DOI: https://doi.org/10.21203/rs.3.rs-1118522/v1

Abstract

Background: Raman and fluorescence spectra techniques are potential tools for disease diagnosis. In recent years, the application of Raman and fluorescence spectra techniques in biological studies has increased a great deal, and clinical investigations relevant to cancer detection by spectroscopic means have attracted particularly attention from both clinical and non-clinical researchers.

Methods: In this article, Raman and fluorescence spectra were employed for the detection of liver cancer and healthy individuals using their serum samples. These serum samples were compared with their spectral features acquired by Raman and fluorescence spectroscopy to initially establish spectral features that can be considered spectral markers of liver cancer diagnosis.

Resuits: The intensity differences from characteristic peaks of carotene, protein and lipid associated Raman spectra were clearly observed in liver cancer patient serum samples versus normal human serum. The changes in the serum fluorescence profiles of liver cancer patients were also analyzed. To probe the capacity and contrast of Raman spectroscopy as an analytical implement for the early diagnosis of liver cancer, principal component analysis (PCA) was used to analyze the Raman spectra of controls , liver cancer patients and healthy individuals. Furthermore, the Partial Least Squares-Discriminant Analysis (PLS-DA) was performed to compare the diagnostic performance of Raman spectroscopy for the classification of disease samples and healthy samples.

Conclusion: Compare with the existing diagnostic techniques, the Raman spectroscopy technique has an excellent advantage in extremely low sample requirements, ease of use and ideal screening procedures. Thus, Raman spectroscopy has great potential to be developed as a powerful tool for distinguishing between healthy and liver cancer serum samples.

1. Introduction

Cancer is a major public health problem worldwide[1, 2]. The latest data from the International Agency for Research on Cancer (IARC)'s World Cancer Report 2020 show that in 2020, there were 19.29 million new cancer cases worldwide, including 10.06 million males and 9.23 million females, and 905,677 new cases of liver cancer accounted for 4.7% of the new cancer, ranking fifth. There were 9.96 million cancer deaths worldwide in 2020, including 5.53 million males and 4.43 million females; of these, 830,180 liver cancer deaths, representing 8.3% of cancer deaths, were ranked third[2–5]. At present, the total treatment condition of liver cancer is still a low radical cure rate, high recurrence rate and poor prognosis. The main reason for the unsatisfactory efficacy of liver cancer is that the diagnosis is late. Approximately 70%~80% of patients with liver cancer have reached the late stage and effective radical treatment cannot be performed. As a result, the early diagnosis of liver cancer is extremely important [4–8]. At present, the monitoring and screening of high-risk groups are the main methods of early diagnosis of liver cancer. Due to the genetic susceptibility of liver cancer, the great differences in morphological diversity and micro-environment and other factors and the rapid development of disease cause the difficult early diagnosis of

liver cancer. For patients with liver cancer, most of them are diagnosed late and unable to cure[5–7]. Using various tests to improve the detection rate has great significance in improving the treatment effect of liver cancer, prolonging patient life and ensuring patient quality of life[6–9].

Currently, the traditional methods for diagnosing liver cancer include ultrasound imaging (US), computed tomography (CT), magnetic resonance imaging (MRI), and detection of serum alpha-fetoprotein (AFP) levels. However, the use of imaging to examine liver cancer is highly dependent on the experience of the operator, and has limited ability to distinguish liver cancer cells. It is a commonly used detection method to diagnose liver cancer by detecting serum AFP content, but the sensitivity of AFP content is very low and cannot be the most effective means for early diagnosis[6–9]. Therefore, it is particularly important to design an economical and simple test method that can quickly and accurately detect and distinguish between early liver cancer patients and normal people. Raman scattering detects the vibrational frequency of molecular chemical bonds, and this intrinsic property makes Raman scattering have ultra-high chemical resolution ability. It is also important in this way, that is, it does not require the addition of external labels to distinguish different components and is a non-labeling technique[10–12]. In the medical field, the occurrence of diseases often starts from subtle variations inside the molecules, which are difficult to detect by routine clinical means, such as changes in the structure of proteins, fats, sugars and nucleic acids[13–15]. However, subtle changes in biological internal molecules can be well detected by Raman spectroscopy, thus providing great guidance and help for the early diagnosis of diseases.

In this paper, the Raman spectra of normal human serum (75 cases) and liver cancer serum (69 cases) were collected. The differences between normal human serum spectra and liver cancer serum spectra were analyzed, and the molecular structure changes of the main components were discussed. The effect of the fluorescence spectrum on Raman spectra was analyzed. The Raman spectra were identified using PCA and PLS-DA, to facilitate the application of Raman spectrum for clinical tumor diagnosis.

2. Materials And Methods

2.1. Raman measurement

Raman spectra were determined by a laser microscopic confocal Raman spectrometer (ANDOR SR-500, UK). The focal length is 500mm, and 1200l/mm grating (Blaze 500) was used in the experiment, and the spectral resolution is 1cm^{-1}. Laser is a 532nm green solid-state laser (Cobolt Samba 532 nm, Cobolt AB Solna, Sweden). A thermoelectric cooled charge-coupled device (CCD) camera is equipped with a back illuminated, deep depletion CDD chip (Andor iDus 416, DU416A LDC-DD, Andor Technology Ltd., Belfast, UK) to collect the sample surface and scattered signals, and cooled the camera to -70°C to reduce noise. Microscope (Leica DM 2700m, Leica microsystems Wetzlar GmbH), 50x (NA=0.5) objective. The edge filter is used to filter stray light. Spectral data were collected using Andor Solis software (Andor Technology).

2.2. Samples preparation

Serum samples were provided by the Department of Thoracic Surgery, the First People's Hospital of Yunnan Province. All participants were informed and signed their consent form for this study. Ethical approval was approved by Biomedical Research Ethics Committee of Yunnan Normal University (No.ynnuethic 2021-14). Serum samples from 69 liver cancer patients and 75 healthy subjects were collected. Sample information is listed in Table 1. Three milliliters of venous blood was drawn from each participant before breakfast and centrifuged at 3000 r/min for 20 min. Then 1.5 mL of upper serum was taken and sealed in an Eppendorf tube and placed in a refrigerator (temperature 4°C) for use. For Raman spectroscopy tests, we used a pipette gun to suck 30 μ l of sample and drop it on a clean glass slide (soak it in aqua regia for 1 h, then wash it with a large amount of ultrapure water, soak it in acetone solution for 1 h, clean it with a large amount of ultrapure water and then blow dry it), and then dry it in the M3 ultraclean chamber.

Table 1
The information of patients with liver cancer and healthy individuals.

	Mean age ± SD	Sex	
		Female (n)	
Patients with liver cancer	55 ± 10	40	29
Healthy individuals	39 ± 12	44	31

2.3. Raman spectral data acquisition and pretreatment

The ANDOR SR-500-type Raman spectrometer laser light path was adjust, a 532 nm excitation wavelength laser was used, and the entire experimental process was performed in the M3 ultraclean chamber laboratory. The spectra were collected by scanning for 15 s and superimposing three times, with a spectral measurement range of 800–1800cm^{-1}, and the spectra in this range covered most of the characteristic Raman peaks of the analytes studied, with a slit width set at 100 microns, to a laser power of approximately 5 mW on the sample. In the acquisition of Raman spectra containing fluorescent substances, fluorescence is an important interference factor, and Raman scattering of serum also has a certain degree of fluorescence interference. Interference caused by fluorescence exists in the acquisition of Raman spectra of serum, so later, we performed fluorescence spectroscopic analysis. To eliminate the spiking effects introduced by cosmic radiation, a running median filter was applied. The entire Raman study flowchart is shown in Figure 1.

2.3. Data analysis

Principal component analysis(PCA) is a widely used multivariate analysis technique that can discriminate Raman spectra originating from biological systems[7,16–22]. All two groups of spectral were simultaneously analyzed using PCA, in order to reduce the spectral dataset to a smaller number of variables (principal components (PCs)) that describe the majority of the variance in the spectral

dataset[16]. Partial least squares discriminant analysis (PLS-DA) is a supervised classification model that is performed on the spectral data of liver cancer and healthy individual samples as X-variables (predictors) and their class information as Y-variables[22–26]. The second derivative spectrum can improve spectral resolution by amplifying small differences[6]. Second derivative Raman spectra were obtained by the Savitzky-Golay algorithm in OMNIC 8.2 software (Thermo Scientific). PCA and PLS-DA analysis of second derivative Raman spectra were performed using Unscrambler X 10.4 software (Camo Software AS, Oslo, Norway).

3. Results And Discussion

3.1. Raman spectra of serum samples

In Fig. 2 shows the Raman spectra of serum samples from 75 healthy individuals. It can be seen from the spectra that the peak positions of the Raman spectra and the Raman spectrum are the same, and the intensity of each Raman peak changes slightly. Considering that the experimental conditions cannot be exactly the same during the test, for example, the laser power of the sample fluctuates slightly due to inconsistent focusing each time, which affects the intensity of the detection signal and moves the spectrum line up and down.

Figure 3 shows the Raman spectra of serum samples from 69 patients with liver cancer. The spectra showed that the Raman spectra of serum samples from patients with liver cancer had the same peak position. The Raman peak intensity of serum from patients with liver cancer was significantly different from the characteristic peak intensity of serum raman spectra from normal subjects. In order to compare the serum Raman spectra of patients with liver cancer and normal subjects, we averaged the spectra shown in Fig. 4(a).

It can be seen from Fig. 4(a) that the Raman characteristic peaks of liver cancer serum and normal serum mainly occurred in the range of 600–1653cm^{-1}. The main Raman peaks are caused by serum proteins, amino acids, lipids, sugars, carbohydrates and other substances, which occurred in the ranges of 745 cm^{-1}, 1003cm^{-1}, 1127cm^{-1}, 1156cm^{-1}, 1301cm^{-1}, 1337cm^{-1}, 1447cm^{-1}, 1519cm^{-1} and 1653cm^{-1}. The peak assignments corresponding to their Raman spectra are shown in Table 2. To find the difference between the serum Raman spectra of liver cancer patients and healthy individuals, differential spectra were found by subtraction as shown in Figure 4(b). In liver cancer patients all component contents were significantly reduced compared with those in healthy individuals. The three peaks with the largest difference are 1003, 1156, and 1519 cm^{-1}, which are due to phenylalanine, protein, carotene, carotenoids and porphyrin content variation[28]. Two high intensity Raman peaks at 1156 and 1519 cm^{-1} due to the resonance raman effect belonging to β-carotene are strongly enhanced under excitation at 532 nm[28, 29]. The decrease in β-carotene in the diseased serum samples is consistent with previous research[29]. In addition, some weak difference Raman peaks appear at 962, 1127, 1297, 1335, 1447, 1584, and 1653cm^{-1} can also be found. The weak differential peaks at 962 cm^{-1} belong to ribose C-O stretching of

ribose[22], 1127 cm^{-1} (C-N stretching Protein), 1297 cm^{-1} (CH_2 deformation Fatty acids), 1335 cm^{-1} (CH_3 CH_2 wagging, collagen (protein assignment), nucleic acid), 1447 cm^{-1} (CH_2 CH_3 bending mode, CH_2 deformation of proteins & lipids), 1584 cm^{-1} (C=C bending mode of phenylalanine)[10], 1653 cm^{-1} (Carbonyl stretch (C=O), C=C stretch Protein amide I absorption)[39, 40]. Patients with malignant tumors are mostly in a high metabolic state, protein synthesis and catabolism in the body are increased, and the metabolites produced and various material components in the blood are also changed. Amino acids are involved in protein synthesis and catabolite, whose composition and concentration can reflect the metabolic state. Hyperproliferation of tumor cells causes changes in protein, amino acids and other components in body fluid. Rapid growth and unlimited proliferation of cancer cells require a large amount of nutritional substrates, especially amino acids, to be consumed, which will inevitably lead to changes in the amino acid metabolic database of cancer tissue.

Table 2
The spectral peaks and their assignments.

Peaks(cm^{-1})	Vibrational mode	Major assignment
745	Symmetrical skeleton stre-tching, T(ring breathing mode of DNA/RNA bases)[30, 10]	Protein, tryptophan[7], Thymine[27]
1003	C-C skeletal	Phenylalanine[30, 10]
1127	C-N stretching[31]	Protein[30],
1156	C-C, C-N stretching	Protein[30], carotenoids, most likely a cellular pigment[32–34],
1230	In-plane vibrations of the conjugated=C-C= [36], β-carotene accumulation (C=C stretch mode)[37]	Glycogen[35]
1301	Antisymmetric stretching vibration[10, 35]	Phosphate[10, 35]
1447	C-H vibration, CH_2 twisting	Triglycerides (fatty acids)[37], Assign from Parker (lipid)[38],
1519	CH_2,CH_3 bending mode,CH_2 deformation	proteins & lipids[10]
1653	C=C stretch mode	porphyrin[10],
1671	C-C & conjugated C=C band stretch	Carotenoid, Carotene[10]
	Carbonyl stretch (C=O), C=C stretch	Protein amide I absorption[39, 40],
	C=C stretching vibrations,	Amide I(anti-parallel β-sheet), Cholesterol & its esters, lipids, fatty acids [10, 37]

3.2. Fluorescence Spectra analysis

Endogenous fluorescent substances are present in the serum, such as proteins, porphyrins, carotenoids, and riboflavin, which can produce fluorescence after excitation by a certain wavelength of light[41–45]. From Fig. 4, we can find that the Raman spectral fluorescence background of liver cancer patients is relatively strong, so we performed fluorescence spectroscopic analysis of the serum of healthy individuals and liver cancer patients. During the experiment, 50 microliters of serum samples were added to 2 ml of saline, diluted and poured into quartz fluorescent colorimetric dishes, put in a fluorescent spectrophotometer (Edinburgh Instruments, FS5 type, UK, with a 150 W xenon lamp as the excitation source, scanning speed of 60nm/min) to obtain physiological saline (background spectroscopy), liver cancer and healthy individual serum fluorescence spectra. The results are shown in Fig. 5. From Fig. 5A, we can see that 462 nm belongs to the fluorescence characteristic peak of physiological saline, with porphyrin luminescence mainly present in the 600-700 nm spectral region[42]. In the spectral region where the largest difference in peak intensity between healthy individuals and liver cancer patients, the molecule playing the main luminescence role is protein[42–46]. Proteins are formed by a peptide chain composed of multiple amino acids repeatedly folding in space, where the amino acids capable of fluorescing are tryptophan, tyrosine, and phenylalanine[43–44]. The growth and division of cancer cells will not be regulated by genes, and their uptake of amino acids is too fast, which disturbs amino acid metabolism in cancer patients, and eventually leads to changes in the content of amino acids in serum[41, 45]. Compared with healthy individuals, liver cancer patients have a reduced ability to degrade aromatic amino acids, and the contents of tryptophan, tyrosine and phenylalanine in serum are significantly increased, with increased concentrations of these three amino acids, leading to enhanced hydrogen bonding energy between light emitting molecules[46–48]. Fluorescence spectra from healthy individual serum and liver cancer patients were used for baseline calibration, and multipeak Gaussian fitting was performed on liver cancer serum (Fig. 5B). We found that the fitted three peaks in the serum of liver cancer patients, 490 nm, 513 nm and 544 nm compared to the three peaks of healthy individuals, 490 nm, 512nm and 580 nm were significantly different in peak position and peak strength. In particular, the peak of serum 544 nm in liver cancer patients was blue-shifted by approximately 36 nm compared with that of healthy individuals 580 nm. This may be due to impaired tissue and organ function in patients with malignant tumors, disrupting amino acid metabolism[45–47]. The content of luminescent amino acids in the free state is increased, and the concentration of amino acids that can emit fluorescence increases, resulting in enhanced hydrogen bond energy and elongation of the two interatomic chemical bonds that form hydrogen bonds[45–47].

3.3. PCA analysis

PCA analysis was performed on the second derivative Raman spectra in range of 1100–1200 cm^{-1} (Fig. 6). Fig. 6a shows that the serum of patients with liver cancer was well separated from the serum samples of healthy individuals. The first three PCs explained 91% of the total variance, with 53% for PC1, 29% for PC2, and 9% for PC3. The loading plot of PCA is used to identify the peaks that make a high

contribution to the differentiated samples. As show in Fig. 6b, PC1 and PC2 mainly contributed greatly near 1127cm^{-1} and 1156 cm^{-1}, which are related to proteins[28] and carotenoids[34–36].

3.4. PLS-DA results

Performed of PLS-DA analysis were make of calibration set (patients with liver cancer provide 52 serum samples and healthy individuals provide 56 serum samples) and validation set (which patients with liver cancer provide 17 serum samples and healthy individuals gave 19 serum samples) according to the ratio of 3:1 for model work in range of 1100–1200 cm^{-1} (Fig. 7). From Fig. 7a, we can see that the serum samples are distributed into two clusters. The red cluster is mainly composed of serum samples from patients with liver cancer, and the blue cluster is mainly composed of the serum samples that healthy individuals gave. Fig. 7b shows the loading plot of Factor-1 and Factor-2 for identifying the peaks with high weights in classifying samples. There are positively weighted peaks at approximately 1158 cm^{-1} and passively weighted peaks at approximately 1154 cm^{-1}. The peak of this region belongs to the Raman peaks of proteins and carotenoids, thus showing that protein and carotenoid changes during liver cancer carcinogenesis dominate in this classification model.

Figure 8 shows the prediction results of PLS-DA in the range of 1100–1200 cm^{-1}. Where predicted Y values greater than zero were considered liver cancer, and less than one was considered healthy. The results showed that the predicted Y values of 17 serum samples from patients with liver cancer and 19 serum samples from healthy individuals were consistent with the actual situation. The effect is very good, and the classification accuracy is 100%

4. Conclusions

Raman and fluorescence spectroscopy were used to classify liver cancer and healthy individual serum samples. The difference spectrum clearly shows the changes in the various major components of the serum in the body during liver carcinogenesis. According to the fluorescence spectroscopy and Raman date analysis of PCA, the main factor causing the serum Raman spectra difference between liver cancer patients and healthy people is the changes of carotenoid and protein in the serum. In particular, fluorescence spectroscopic analysis found that the amino acid content that shines freely under the influence of malignant tumors increases (including tryptophan, tyrosine, and phenylalanine), which can provide a reference for clinical treatment. Using Raman spectroscopic data, a PLS-DA model was established to accurately classify serum samples from healthy individuals and liver cancer patients. Based on Raman spectroscopy, we currently well distinguish a limited sample of liver patients and healthy individuals. Although further studies are needed to clearly explain the characteristic Raman spectra of various serum biomolecules, the results obtained are very promising to use Raman spectroscopy for clinical diagnosis. Significantly, compare with the existing diagnostic techniques, the Raman spectroscopy technique has an excellent advantage in extremely low sample requirements, ease of use and ideal screening procedures. It can provide a clear and objective result at the molecular level

and help reduc the human errors on the objective result to the maximum. Thus, Raman spectroscopy has great potential to be developed as a powerful tool for distinguishing between healthy and liver cancer serum samples.

Declarations

Acknowledgements

None.

Authors' contributions

QO and XY performed study concept, design, development of methodology and writing; WY and GL performed technical, review and revision of the paper; LJ and YM provided acquisition, analysis and interpretation of data, and statistical analysis; KQ provided material support. All authors read and approved the final paper.

Funding

This work was supported by the National Natural Science Foundation of China (Grant No. 31760341), Yunnan province University Science and Technology Innovation Team Support Scheme. The authors are grateful for these financial supports.

Availability of data and materials

The datasets used and/or analysed during the current study available from the corresponding author on reasonable request.

Ethics approval and consent to participate

Ethical approval was approved by Biomedical Research Ethics Committee of Yunnan Normal University prior to commencing this study (No.ynnuethic 2021-14). All methods were carried out in accordance with relevant guidelines and regulations, and informed consent was obtained from all participants.

Consent for publication

Not applicable.

Competing interests

The authors declare that they have no competing interests.

References

1. Siegel, R. L., Miller, K. D., Jemal, A. Cancer statistics, 2020. *CA Cancer J Clin* **2020**, 70, (1), 7-30. http://doi.org/10.3322/caac.21590
2. Cheristopher P. Wild, Elisabete Weiderpass, Bernard W. Stewart. World Cancer report: cancer research for cancer prevention, Lyon, 2020. https://www.iarc.who.int/featured-news/new-world-cancer-report/
3. Torre, L.A., Bray, F., Siegel, R.L., Ferlay, J., Lortet-Tieulent, J. and Jemal, A. Global Cancer Statistics, 2012. CA: A Cancer Journal for Clinicians, 2015; 65(2): 87–108. https://doi.org/10.3322/caac.21262
4. Anwanwan, D., Singh, S. K., Singh, S., Saikam, V., Singh, R. Challenges in liver cancer and possible treatment approaches. *Biochim Biophys Acta Rev Cancer* 2020, 1873, (1), 188314. http://doi.org/10.1016/j.bbcan.2019.188314
5. Hartke, J.; Johnson, M.; Ghabril, M., The diagnosis and treatment of hepatocellular carcinoma. *Semin Diagn Pathol* 2017, 34, (2), 153–159. http://doi.org/10.1053/j.semdp.2016.12.011
6. Yang, X.; Ou, Q.; Yang, W.; Shi, Y.; Liu, G., Diagnosis of liver cancer by FTIR spectra of serum. *Spectrochim Acta A Mol Biomol Spectrosc* **2021**, 263, 120181. http://doi.org/10.1016/j.saa.2021.120181
7. Zhang, K.; Hao, C.; Man, B.; Zhang, C.; Yang, C.; Liu, M.; Peng, Q.; Chen, C., Diagnosis of liver cancer based on tissue slice surface enhanced Raman spectroscopy and multivariate analysis. *Vibrational Spectroscopy* 2018, 98, 82–87. http://doi.org/10.1016/j.vibspec.2018.07.010
8. Liu, K.; Jin, S.; Song, Z.; Jiang, L.; Ma, L.; Zhang, Z., Label-free surface-enhanced Raman spectroscopy of serum based on multivariate statistical analysis for the diagnosis and staging of lung adenocarcinoma. *Vibrational Spectroscopy* 2019, 100, 177–184. http://doi.org/10.1016/j.vibspec.2018.12.007
9. Lennon A M, Buchanan A H, Kinde I, et al. Feasibility of blood testing combined with PET-CT to screen for cancer and guide intervention. Science, 2020, 369(49):eabb9601. DOI: 10.1126/science.abb9601
10. Movasaghi, Z.; Rehman, S.; Rehman, I. U., Raman Spectroscopy of Biological Tissues. *Applied Spectroscopy Reviews* 2007, 42, (5), 493–541. http://doi.org/10.1080/05704920701551530
11. T.Bhattacharjee, G. Maru, A. Ingle, C. Murali Krishna, Transcutaneous in vivo Raman spectroscopy of breast tumors and pretumors. Journal of Raman Spectroscopy, 2015, 46, 1053–1061.
12. Paraskevaidi, M.; Ashton, K. M.; Stringfellow, H. F.; Wood, N. J.; Keating, P. J.; Rowbottom, A. W.; Martin-Hirsch, P. L.; Martin, F. L., Raman spectroscopic techniques to detect ovarian cancer biomarkers in blood plasma. *Talanta* 2018, 189, 281–288. http://doi.org/10.1016/j.talanta.2018.06.084
13. Wen, W.; Meng, Y.; Xiao, J.; Zhang, P.; Zhang, H., Comparative study on keratin structural changes in onychomycosis and normal human finger nail specimens by Raman spectroscopy. *Journal of Molecular Structure* **2013**, 1038, 35–39. http://doi.org/10.1016/j.molstruc.2013.01.051
14. Palonpon A F, Ando J, Yamakoshi H, et al, Raman and SERS microscopy for molecular imaging of live cells, Nature Protocols, 2013, 8(4): 677–692.

15. Pal S, Ray A, Andreou C, et al. DNA-enabled rational design of fluorescence-Raman bimodal nanoprobes for cancer imaging and therapy. Nature Communications, 2019,10(1): 1926.
16. Harder, S. J. et al. Raman spectroscopy identifies radiation response in human nonsmall cell lung cancer xenografts. Sci. Rep. 6, 21006; doi: 10.1038/srep21006 (2016).
17. Yan S, Wang S, Qiu J, et al. Raman spectroscopy combined with machine learning for rapid detection of food-borne pathogens at the single-cell level. Talanta, 2021, 226,122195.
18. Zheng C, Qing S, Wang J, et al. Diagnosis of cervical squamous cell carcinoma and cervical adenocarcinoma based on Raman spectroscopy and support vector machine. Photodiagnosis and Photodynamic Therapy, 2019, 27, 156–161. http://doi.org/10.1016/j.pdpdt.2019.05.029
19. Wang H, Chen C, Tong D, et al. Serum Raman spectroscopy combined with multiple algorithms for diagnosing thyroid dysfunction and chronic renal failure. Photodiagnosis and Photodynamic Therapy, 2021,34,102241.
20. Kemmlera M, Rodner E, Rösch P, et al. Automatic identification of novel bacteria using Raman spectroscopy and Gaussian processes, Analytica Chimica Acta, 2013, 794, 29–37.
21. Cordovana M, Mauder N, Kostrzewa M, et al. Classification of Salmonella enterica of the (Para-)Typhoid Fever Group by Fourier-Transform Infrared (FTIR) Spectroscopy. Microorganisms, 2021, 9(4): 853.
22. Nargis H.F., Nawaz H., Bhatti H. N., et al. Comparison of surface enhanced Raman spectroscopy and Raman spectroscopy for the detection of breast cancer based on serum samples. Spectrochimica Acta Part A Molecular and Biomolecular Spectroscopy, 2021, 246: 119034.
23. Bahreini M, Hosseinzadegan A, Rashidi A, et al, A Raman-based serum constituents' analysis for gastric cancer diagnosis: In vitro study. *Talanta* 2019, 204, 826–832. http://doi.org/10.1016/j.talanta.2019.06.068
24. Meutter J D, Goormaghtigh E. FTIR Imaging of Protein Microarrays for High Throughput Secondary Structure Determination. Analytical Chemistry, 2021, 93(8): 3733–3741. https://doi.org/10.1021/acs.analchem.0c03677.
25. Xia L, Lu J, Chen Z, et al. Identifying benign and malignant thyroid nodules based on blood serum surface-enhanced Raman spectroscopy. Nanomedicine: Nanotechnology, Biology, and Medicine, 2021,32 ,102328.
26. Zhang K, Liu X, Man B, et al. Label-free and stable serum analysis based on Ag-NPs/PSi surface-enhanced Raman scattering for noninvasive lung cancer detection. Biomedical Optics Express, 2018, 9(9):4345–4358.
27. Xiao R, Zhang X, Rong Z, et al. Non-invasive detection of hepatocellular carcinoma serum metabolic profile through surface-enhanced Raman spectroscopy. Nanomedicine: Nanotechnology, Biology, and Medicine, 2016, 12: 2475–2484. http://dx.doi.org/10.1016/j.nano.2016.07.014.
28. Zheng X, Wu G, Lv G, et al. Combining derivative Raman with autofluorescence to improve the diagnosis performance of echinococcosis. Spectrochim. Acta A, 2021, 247, 119083.

29. Ullah R, Khan S, et al., Demonstrating the application of Raman spectroscopy together with chemometric technique for screening of asthma disease, Biomed. Opt. Express, 2019, 10(2): 600–609.
30. James W. Chan, Douglas S. Taylor, Theodore Zwerding, et al. Micro-Raman Spectroscopy Detects Individual Neoplastic and Normal Hematopoietic Cells. Biophysical Journal, 2006, 90(2):648–656.
31. Jyothi Lakshmi R, Kartha V. B, Murali Krishna C., et al. Tissue Raman spectroscopy for the study of radiation damage: brain irradiation of mice. Radiation Research, 2002, 157(2):175–182.
32. Mahadevan-Jansen A, Richards-Kortum R. Raman spectroscopy for cancer detection: a review. Proceedings of the 19th Annual International Conference of the IEEE Engineering in Medicine and Biology Society. *'Magnificent Milestones and Emerging Opportunities in Medical Engineering' (Cat. No.97CH36136)*, 1997, 6: 2722-2728. https://ieeexplore.ieee.org/document/756895/authors#authors.
33. Stone N, Kendall C, Smith J, et al. Raman spectroscopy for identification of epithelial cancers. Faraday Discussions, 2004, 126:141–157
34. Stone N, Kendall C, Shepherd N, et al. Near-infrared Raman spectroscopy for the classification of epithelial pre-cancers and cancers. Journal of Raman Spectroscopy, 2002, 33:564–573. https://doi.org/10.1002/jrs.882
35. Dukor R K. Vibrational Spectroscopy in the Detection of Cancer. Handbook of Vibrational Spectroscopy, 2006. https://doi.org/10.1002/0470027320.s8107.
36. Puppels G. J., Garritsen H.S.P., Kummer J.A., et al. Carotenoids located in human lymphocyte subpopulations and natural killer cells by Raman microspectroscopy. Cytometry, 1993, 14(3):251–256.
37. Landulfo Silveira, Jr., Sokki Sathaiah, Renato A. Zângaro, et al. Correlation between near-infrared Raman spectroscopy and the histopathological analysis of atherosclerosis in human coronary arteries. Lasers in Surgery and Medicine, 2002, 30(4):290–297. https://doi.org/10.1002/lsm.10053
38. Malini R., Venkatakrishna K., Kurien J., et al. Discrimination of normal, inflammatory, premalignant, and malignant oral tissue: A Raman spectroscopy study. Biopolymers, 2006, 81(3):179–193.
39. Farquharson S, Shende C, Inscore F E., et al. Analysis of 5-fluorouracil in saliva using surface-enhanced Raman spectroscopy. Journal of Raman Spectroscopy, 2005, 36(3):208–212.
40. Frank C J., Mccreery R L., Redd D. C. B. Raman spectroscopy of normal and diseased human breast tissues. Analytical Chemistry, 1995, 67(5):777–783.
41. Guan C., Luo X., Lu J., Li Z. The study of the peak position blue shift and molecular vibration mechanism of serum fluorescence spectra in mice with liver cancer. Journal of Optoelectronics ·laser, 2019, 30(2): 221–226. https://doi.org/10.16136/j.joel.2019.02.0209
42. Yu J., Meng J., Ma J., Zheng R., Fluorescence Study by Simulating the Metabolizability of Carotenoid and Porphyrin during Cancer Development. Spectroscopy and Spectral Analysis, 2001, 24(8):981–983. https://doi.org/10.1016/j.jco.2003.08.015

43. Albani J. R., Origin of Tryptophan Fluorescence Lifetimes Part 1. Fluorescence Lifetimes Origin of Tryptophan Free in Solution. Jounal of Fluorescence, 2014, 24: 93–104. https://doi.org/10.1007/s10895-013-1277-8
44. Masilamani V., Al-Zhrani K., Al-Salhi M., Al-Diab A., Al-Ageily M. Cancer diagnosis by autofluorescence of blood components. Journal of Luminescence, 2004, 109: 143–154. https://doi.org/:10.1016/j.jlumin.2004.02.001
45. Scheiner S., Kar T., Pattanayak J. Comparison of Various Types of Hydrogen Bonds Involving Aromatic Amino Acids. Journal of the American Chemical Society, 2002, 124(44): 13257–13264. https://doi.org/10.1021/ja027200q
46. Joseph J., Jemmis E D. Red-, Blue-, or No-Shift in Hydrogen Bonds: A Unified Explanation. Journal of the American Chemical Society, 2007, 129(15): 4620–4632. https://doi.org/10.1021/ja067545z
47. Masilamani V., AlSalhi M S., Vijmasi T., Govindarajan K., Rai R R., Atif M., Prasad S., Aldwayyan A S. Fluorescence spectra of blood and urine for cervical cancer detection. Journal of Biomedical Optics, 2012, 17(9): 098001. https://doi.org/10.1117/1.JBO.17.9.098001
48. Croce A.C., Bottiroli G. Autofluorescence spectroscopy and imaging: a tool for biomedical research and diagnosis. European Journal of Histochemistry, 2014, 58:2461. https://doi.org/10.4081/ejh.2014.2461

Figures

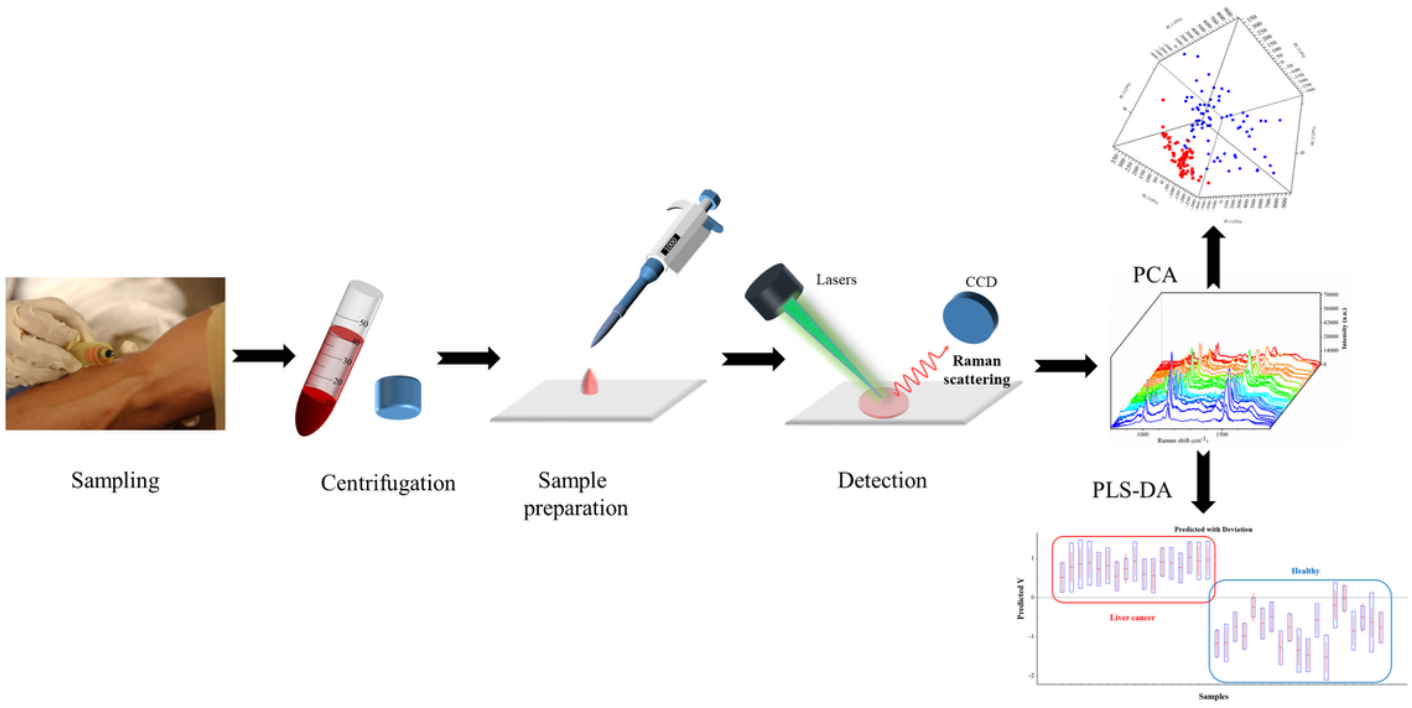

Figure 1

Flow chart of Raman spectroscopy acquisition and analysis of serum samples

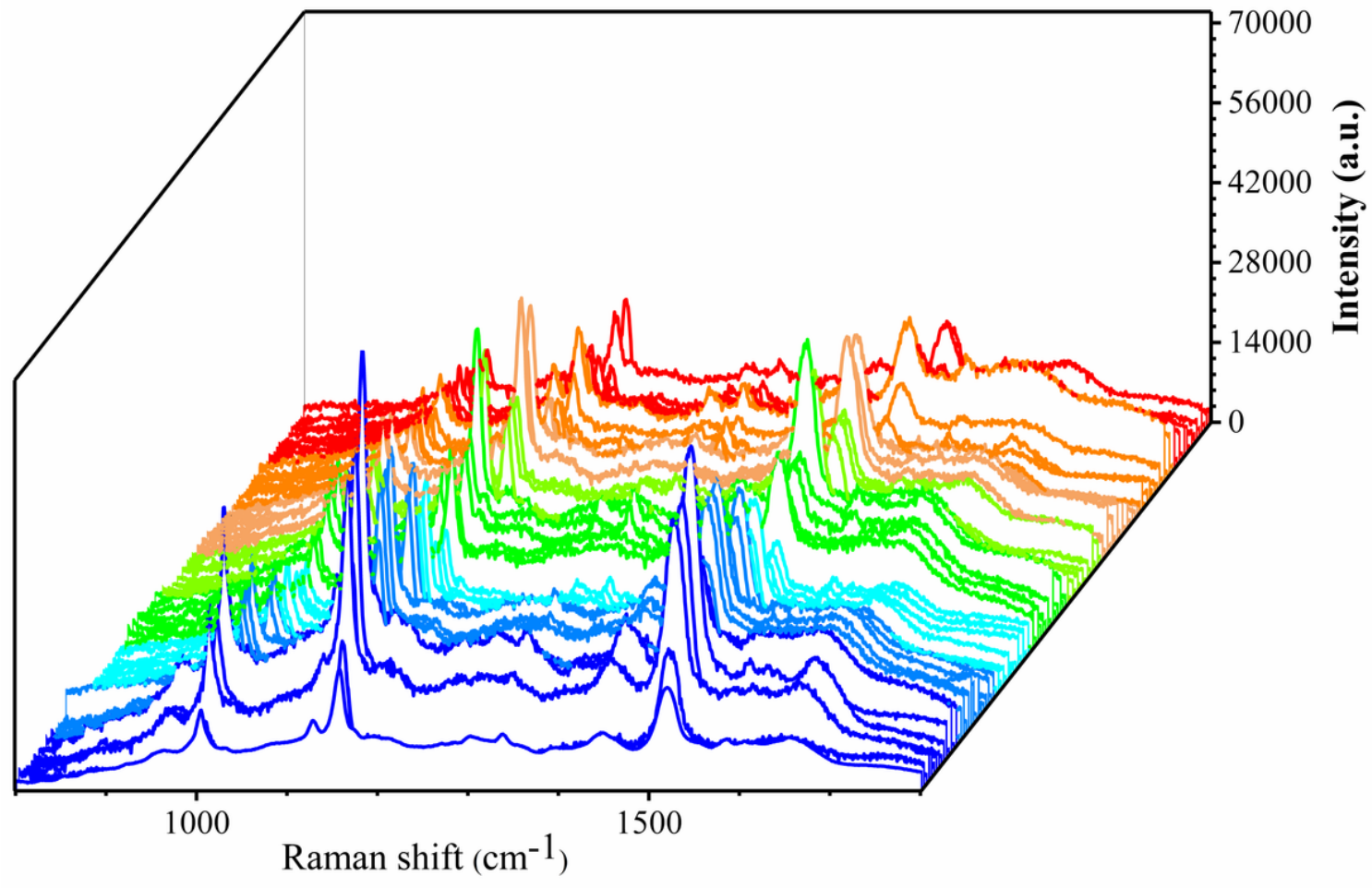

Figure 2

Raman spectra of serum samples from 75 healthy individuals.

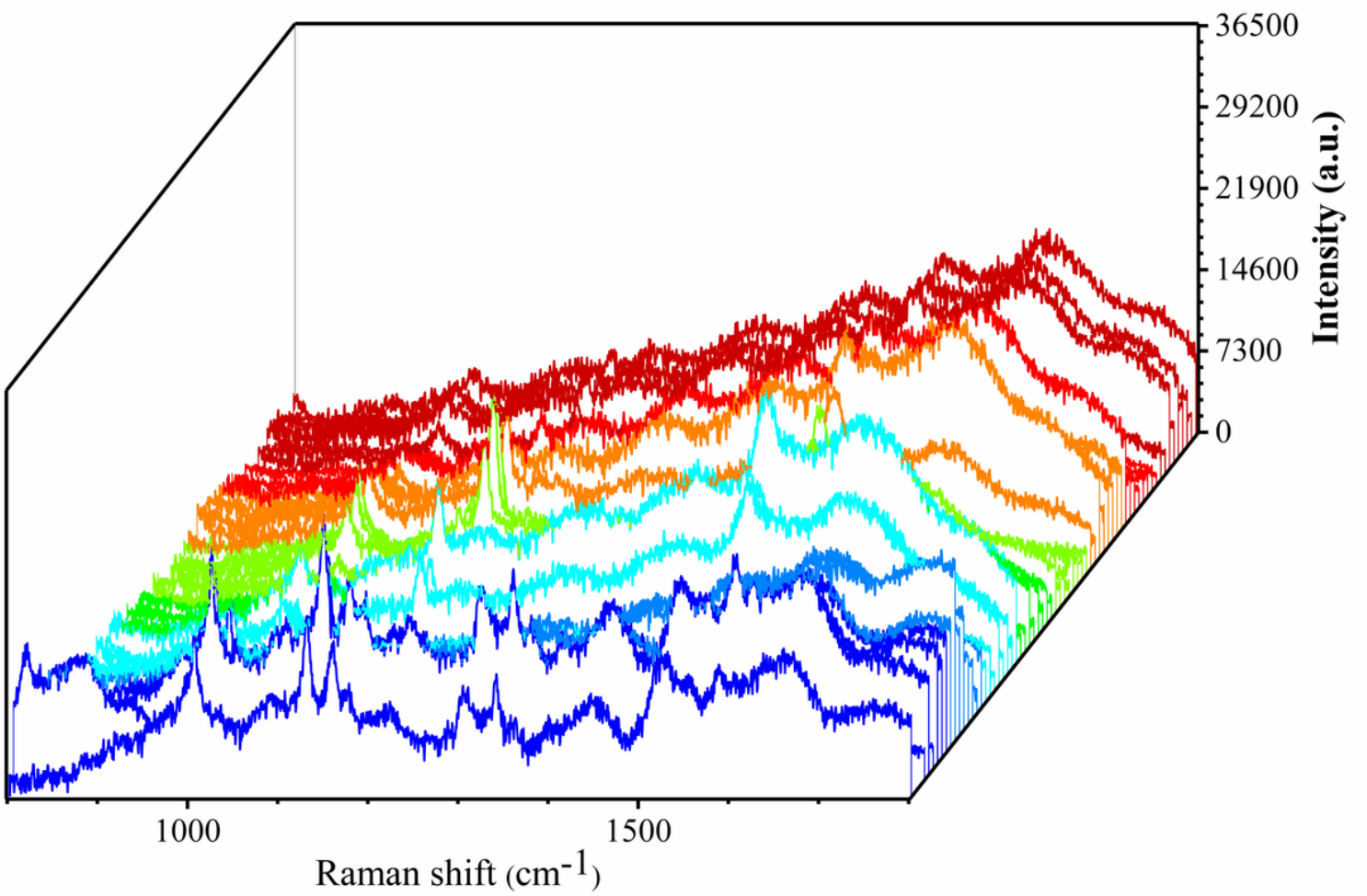

Figure 3

Raman spectra of serum samples from 69 patients with liver cancer.

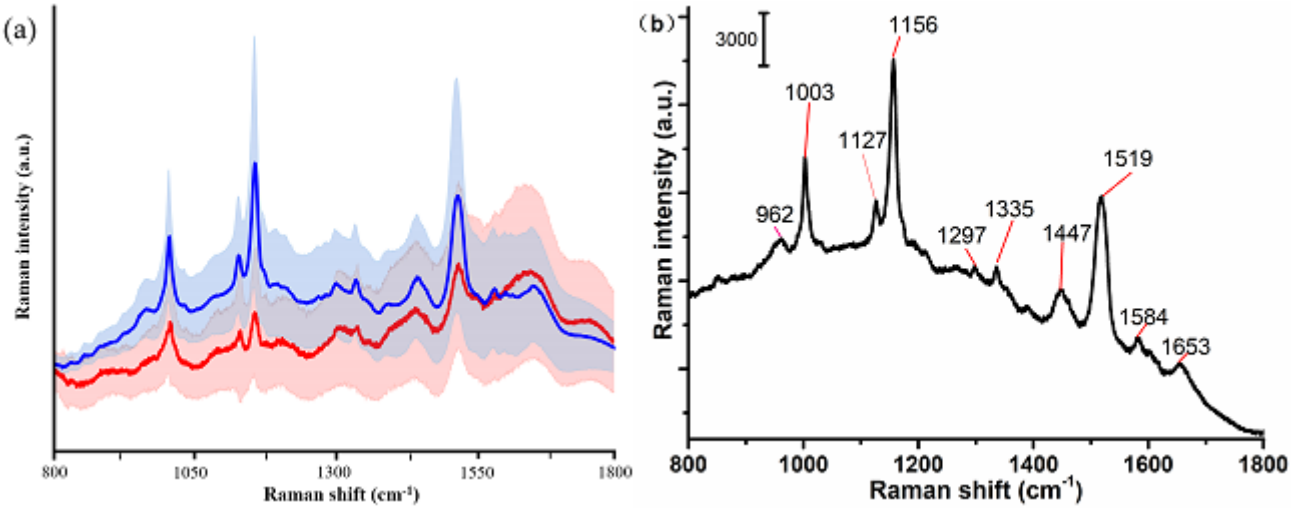

Figure 4

(a) Average Raman spectra of serum from patients with liver cancer (red line, n=69) and healthy individuals (blue line, n=75). The shaded portion indicates the standard deviation. (b) The difference spectrum between liver cancer and healthy individuals.

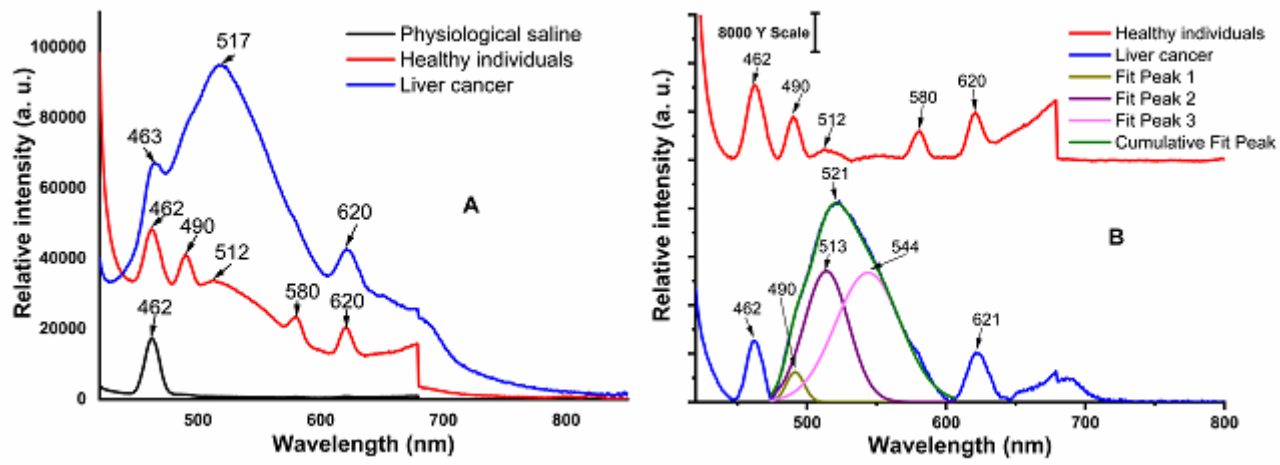

Figure 5

A, Fluorescent spectra of serum from healthy individuals and liver cancer patients**. B,** Baseline calibrationg fluorescent spectra and liver cancer serum multipeak Gaussian fitting fluorescent spectra.

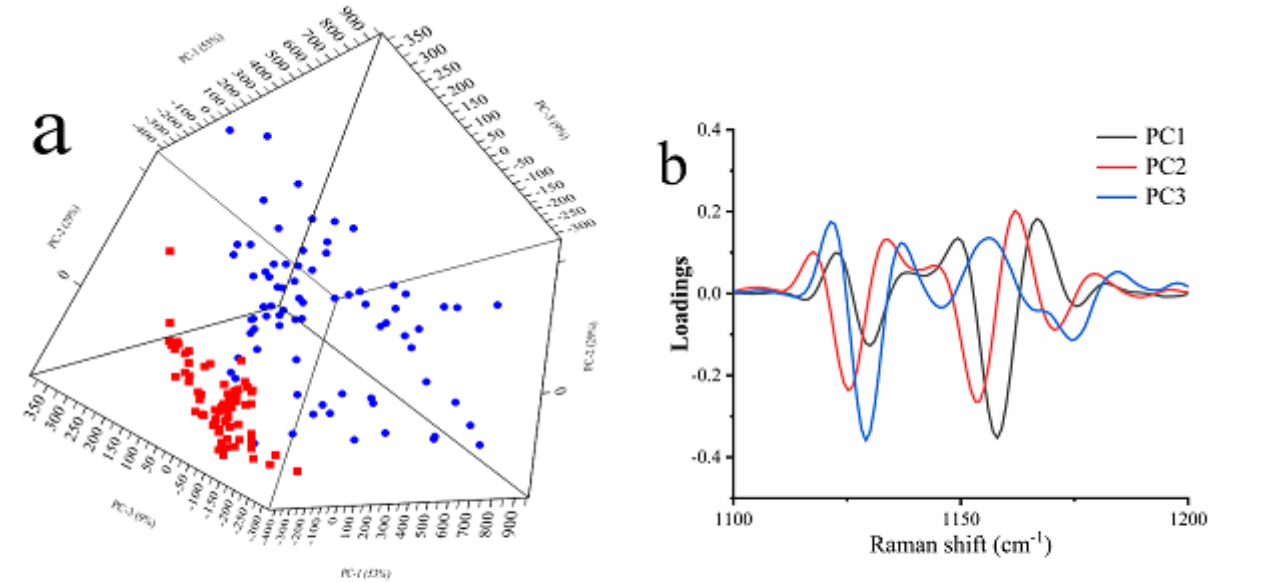

Fig. 6. PCA analysis results in range of 1100–1200 cm^{-1}. Scatter plot of PCA (a) and loading plot (b) on the second derivative Raman spectra in the range of 1100–1200 cm^{-1}: ■ serum from patients with liver cancer, ● serum from healthy individuals.

Figure 6

See image above for figure legend

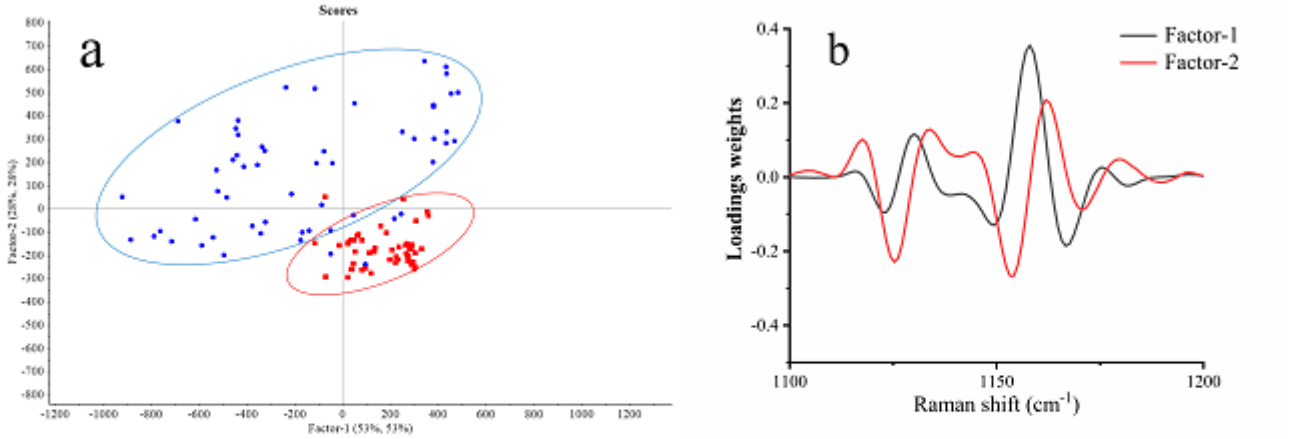

Fig. 7. PLS-DA results in range of 1100–1200 cm^{-1}. Scatter plot of PLS (a) and loading weights (b) on the second derivative Raman spectra in the range of 1100–1200 cm^{-1}: ■ serum from patients with liver cancer, ● serum from healthy individuals.

Figure 7

See image above for figure legend

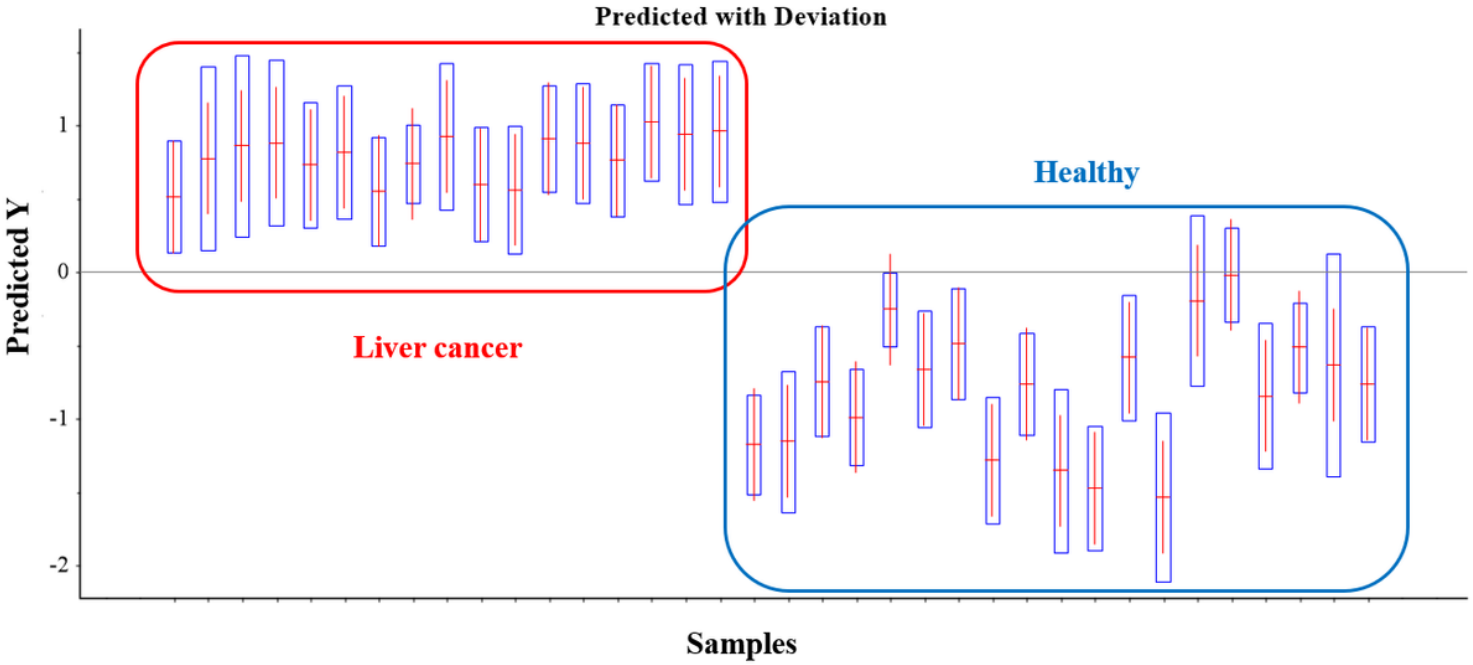

Figure 8

Prediction results of PLS-DA in the range of 1100–1200 cm^{-1}.